Computational Efforts in Designing Experiment for High-lift Aeroacoustics

Mitsuhiro Murayama
Yuzuru Yokokawa
Kazuomi Yamamoto
Yasushi Ito

Aviation Program Group, Japan Aerospace Exploration Agency
7-44-1 Jindaiji-Higashi, Chofu, Tokyo 182-8522
Japan
murayama.mitsuhiro@jaxa.jp, yokokawa.yuzuru@jaxa.jp, yamamoto.kazuomi@jaxa.jp, ito.yasushi@jaxa.jp

Kazuhisa Amemiya

Advanced Science & Intelligence Research Institute
1-18-14 Uchikanda, Chiyoda-ku, Tokyo 101-0047
Japan
amemy@chofu.jaxa.jp

Kentaro Tanaka
Tohru Hirai

Ryoyu Systems Co., Ltd.
2-19-13 Takanawa, Minato-ku, Tokyo 108-0074
Japan
kentaro@chofu.jaxa.jp, thirai@chofu.jaxa.jp

Abstract

In this paper, computational efforts in designing experiment for a series of wind tunnel tests of high-lift airframe noise measurement and the importance are shown. This paper describes computational evaluations of the design of wind tunnel testing model, the model sizing and mounting in wind tunnel, and influences of shear layer and mounted plate on the sound propagation in open-cart test section. It is shown that preliminary CFD investigation of the wind tunnel tests can decrease unknowns and improve the accuracy of the wind tunnel test.

Key words: high-lift, aeroacoustics, computational fluid dynamics, wind tunnel test

Introduction

With recent interest in the environmental problems, regulations for aircraft noise around airports have tightened. Due to successive efforts for noise reduction from aircraft engines, airframe noise is getting prominent for the overall noise level, especially during approach where engines are throttled down. Therefore, noise reduction technologies for the airframe noise are getting important for developments of future commercial aircraft. The

noise from high-lift devices deployed during landing and take-off such as leading-edge slat and trailing-edge flap is known as one of major noise sources of the airframe noise besides the noise from landing gears [1-3].

Recent progresses of CFD technologies solving Reynolds-Averaged Navier-Stokes (RANS) equations and computer resources have improved the accuracy to predict the steady-state aerodynamics phenomena and performance to a useful level applicable in the design process, even for full-aircraft configurations deployed high-lift devices [4-6]. In recent years, efforts to validate and improve CFD/CAA (Computational AeroAcoustics) for airframe noise computations have been promoted internationally through several workshops such as BANC (Workshop on Benchmark problems for Airframe Noise Computations) [7-8]. However, the daily use of CFD/CAA to simulate the noise from high-lift devices especially for full aircraft configurations still requires to solve several difficulties in the grid generation, prediction accuracy and computational resources. The airframe noise research still relies largely on wind tunnel testing, collaborating with numerical simulations. JAXA has conducted research work using a series of wind tunnel tests and numerical simulations on the noise generation mechanism and reduction technologies around the high-lift devices and landing gears [9-15]. To investigate the airframe noise from high-lift devices, several research models such as a simple rectangular single wing model and a realistic wing-fuselage model deployed high-lift devices have been used for the wind tunnel tests and numerical simulations [6, 16-17]. The research using the most complicated wing-fuselage model deployed high-lift devices with an engine nacelle, which is the wind tunnel testing model basically for aerodynamic test purpose, had tried to identify the noise sources and characteristics generated from the realistic aircraft configurations such as slat side-edges. On the other hand, dimensions of slat and flap are small in the half-span wind tunnel testing model of complete aircraft configuration with 2.3m half-span length. The flowfields are complicated with interferences of engine-nacelle. They made it difficult to investigate the detail flowfields around identified noise sources and basic noise characteristics from each component. The research using a simplified three-dimensional high-lift wing model, “OTOMO”, shown in Fig. 1 had clarified the details of noise characteristics and generation mechanisms from high-lift devices [9-15]. The studies using the models had improved techniques of the wind tunnel tests such as noise source identification using phased-array microphones and flow visualization using PIV and numerical simulation methods such as LES and LES/RANS hybrid method. In addition, the devices and concepts to reduce the noise have been also proposed and validated using the models.

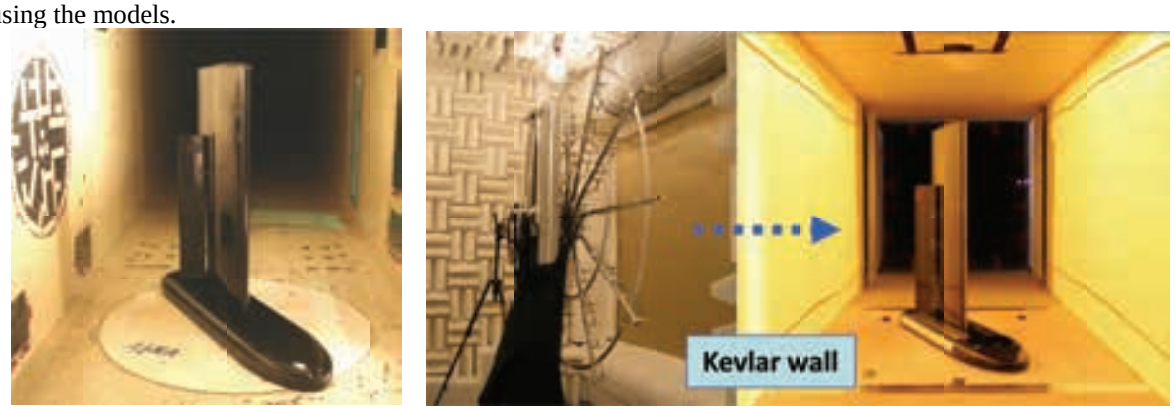

(i) Solid-wall cart (ii) Anechoic Kevlar-wall cart

(a) 2m × 2m JAXA-LWT2

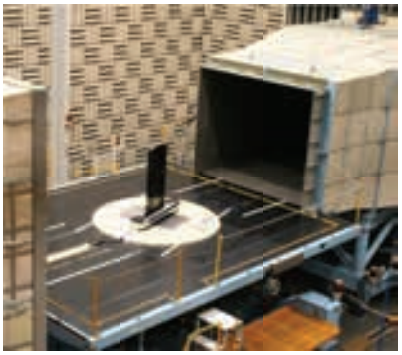

(b) 3m × 2.5m Large-Scale Anechoic Wind Tunnel in Railway Technical Research Institute

Fig. 1 JAXA high-lift device noise research model, “OTOMO” mounted in the wind tunnel facilities [9-15]

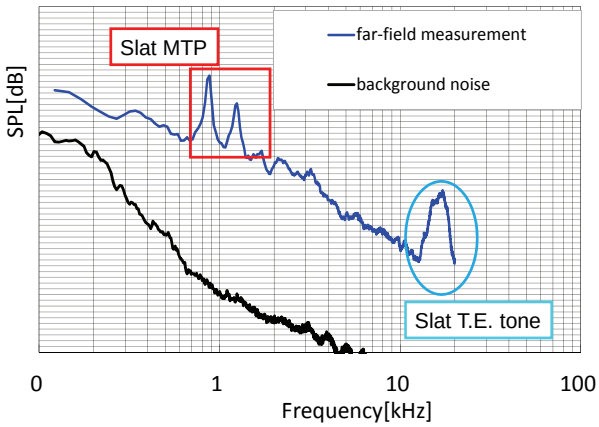

Fig. 2 Example of narrow-band spectra of far-field SPL of OTOMO model [11]

The research model shown in Fig. 1 employed a rectangular wing planform and omitted the sweep angle, taper, and dihedral angle. Toward further improvements to predict and reduce the airframe noise from actual aircrafts, the influences of the omitted parameters on the noise generation mechanisms and the effectiveness of devices and concepts to reduce noise should be investigated well. For example, in several wind tunnel test results such as two-dimensional wind tunnel test results and test results using JAXA's rectangular high-lift wing model [11], Multiple Tonal Peaks (MTPs) generated from slat are observed as shown in Fig. 2. On the other hand, it has been said that MTPs are not necessarily observed in flight test results. In addition, noise sources are often identified around detail parts such as slat tracks and cavities in flight test results of actual aircrafts, which are specific in the actual aircrafts and not modeled or simplified in the wind tunnel testing model. The influences of such detail parts in actual aircrafts should be also clarified for further improvements to predict and reduce the airframe noise from actual aircrafts.

To investigate the influences, a half-span three-element high-lift wing model with taper and sweep angle were designed and fabricated for the purpose of high-lift device noise research. A series of wind tunnel tests have been conducted since 2011. In this paper, the computational efforts in designing experiment for the wind tunnel tests and its importance are shown. For successful wind tunnel tests of high-lift device noise research, preliminary CFD investigation of the wind tunnel tests can decrease unknowns and improve the accuracy of the wind tunnel test. The preliminary CFD results help to appropriately and efficiently locate steady/unsteady pressure sensors to be measured. The model has to be appropriately designed to simulate expected flowfields and conditions in the wind tunnels. The model sizing and mounting method should be carefully selected to avoid strong wind tunnel interference at high-lift conditions. In the case of open-cart test to evaluate far-field noise, careful consideration is required. If the model generates unexpected extra noise, it is difficult to distinguish the influence from the measured spectra. In addition, in the case of open-cart test, generated shear-layers largely deflect due to high-lift. The deflected flow has to be in the collector without generating extra noise at the required conditions. For the purpose of high-lift device noise research, not only the wind tunnel data correction for aerodynamic forces, but also the influence on the sound propagation through the deflected shear-layers and sound reflection on the mounted plate should be evaluated.

Designed Wind Tunnel Testing Model for High-lift Device Noise Research, OTOMO2

The model is designed to have a leading-edge slat and a trailing-edge single-slotted flap assuming an outer wing with sweep angle of a 100-passenger-class civil jet aircraft. The designed model configuration, OTOMO2, is shown in Fig. 3.

Noise sources around slat are mainly derived from unsteadiness of the shear layers from the cusp and the slat trailing edge. Three noise components have been observed up to now [11]. The first component is the low frequency broadband component. The second component is the multiple tonal peaks (MTP) superimposed on

the low frequency broadband component. The third component, high frequency tone noise, is governed by the Karman vortex shedding from the trailing edge of the slat. Several other possibilities are the slat tracks, the cavities around the slat track, and anti-icing vent. In addition, to seal gaps between slat and the leading-edge of the main wing when the slats are stowed at the cruise conditions, blade seal and bulb seal are often attached as shown in Fig. 4. They change the shear layers from the cusp and the flow pattern in the cove. Besides the basic characteristics of noise from slat, the influences of such detail parts in actual aircrafts should be also clarified for further improvements to predict and reduce the airframe noise from actual aircrafts. This model is designed to allow the additional evaluation of the influences. Figure 5 shows the examples of additional parts of simulated slat tracks and cavities.

As for noise from flap, flap side-edge is recognized to be a major noise source. The noise sources at the flap-edge were clarified as three main sources; noise at low-frequency around the aft of flap trailing edge by vortex instability, broadband noise at mid-frequency around the side-edge of flap by shear-layer instability, and broadband noise at high-frequency around the gap between main wing and flap by shear-layer instability [18-19]. In this model, flap-tip region is designed to be exchangeable. As for the flap track, a flap track fairing can be evaluated as shown in Fig. 6.

Two CFD codes had been used to design the model. One is a flow solver on multi-block structured grids, UPACS, which is a standard CFD code for multi-block structured grids in JAXA [20-23]. The other one is a flow solver on unstructured grids, TAS code [20, 24], which is one of major CFD codes for unstructured grids used in APG/JAXA. The mixed element unstructured grids composed of tetrahedrons, prisms, and pyramids for viscous flows with high Reynolds number were generated using unstructured surface/volume mesh generators, TAS-Mesh and MEGG3D [25-29].

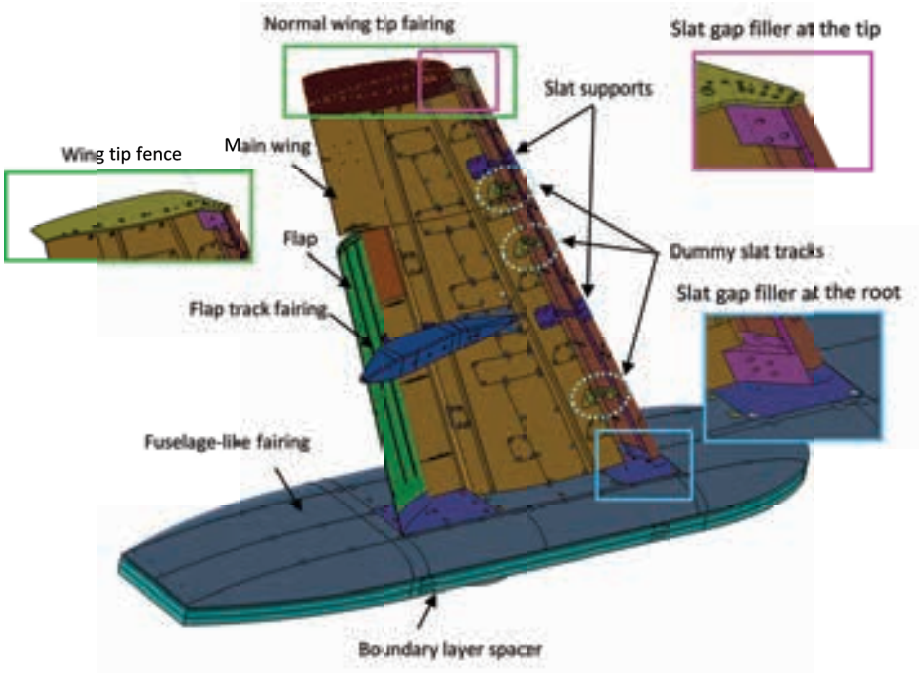

Fig. 3 Designed JAXA high-lift device noise research model with taper and sweep angle, "OTOMO2"

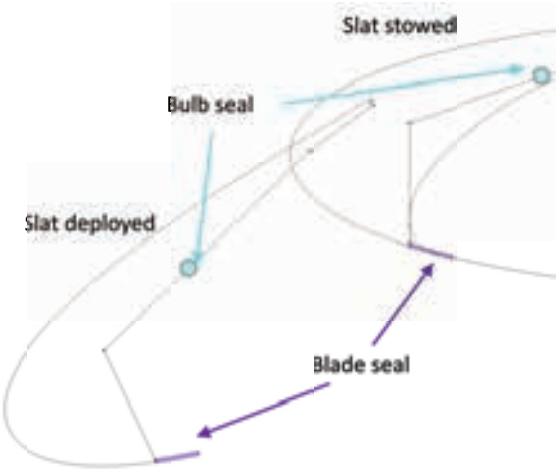

Fig. 4 Schematic of blade seal and bulb seal

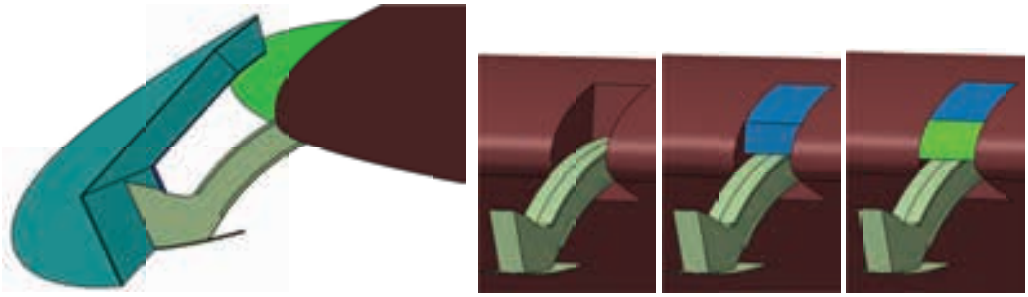

Fig. 5 Examples of additional parts of simulated slat tracks and cavities in the wind tunnel test model

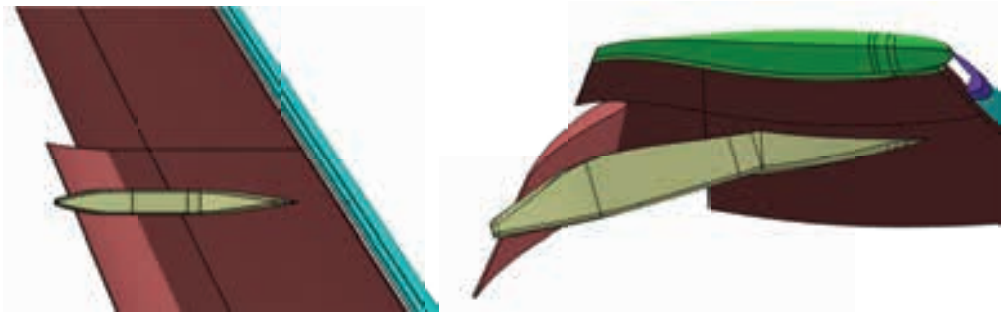

Fig. 6 Simulated flap track fairing in the wind tunnel test model

Design of Wing Geometry

In this research, use of two different wind tunnel facilities is assumed. One is the JAXA-LWT2 Lowspeed Wind Tunnel shown in Fig. 1(a). The facility is used for measurements of noise source identification by microphone phased-array, aerodynamic force and moment, static/unsteady pressure, and flowfield by oil-flow and PIV. It is an atmospheric pressure closed-circuit tunnel with a solid wall square test section or a Kevlar wall square test section. The size of the test section is 2m in height, 2m in width, and 4m in length. The other one is the Large-Scale Anechoic Wind Tunnel in Railway Technical Research Institute (RTRI) [30] shown in Fig. 1(b). The tunnel has an open-jet nozzle with a rectangular cross-section. The size of the test section is 3m in width, 2.5m in height, and 8m in length. The facility is used for measurements of far-field noise spectra including directivity characteristics, aerodynamic force and moment, and static/unsteady pressure. In order to investigate details of noise sources, the model size is designed to be maximized in the wind tunnels.

To be consistent with a series of JAXA's high-lift noise researches, the wing geometry is designed based on two models, a realistic aircraft wing-fuselage model deployed high-lift devices, JSM (JAXA Standard Model) [6, 16-

17], shown in Fig. 7 and a simplified high-lift model, OTOMO, shown in Fig. 1. The wing planform is based on the outer wing of JSM. The half-span length should be less than 1.5m in the JAXA-LWT2 for high-lift configuration. The half-span length of JSM is 2.3m. To be full-span slat and 70%span flap, the wing planform of from 54% to 88% span is used for the baseline planform. The stowed section airfoil and the setting parameter of slat and flap are identical with those of OTOMO. The slat and flap are deployed in three-dimensional direction based on the wing planform to evaluate under realistic aircraft situations. The differences of flowfields by the deployment methods are preliminary evaluated by CFD as shown in Fig. 8.

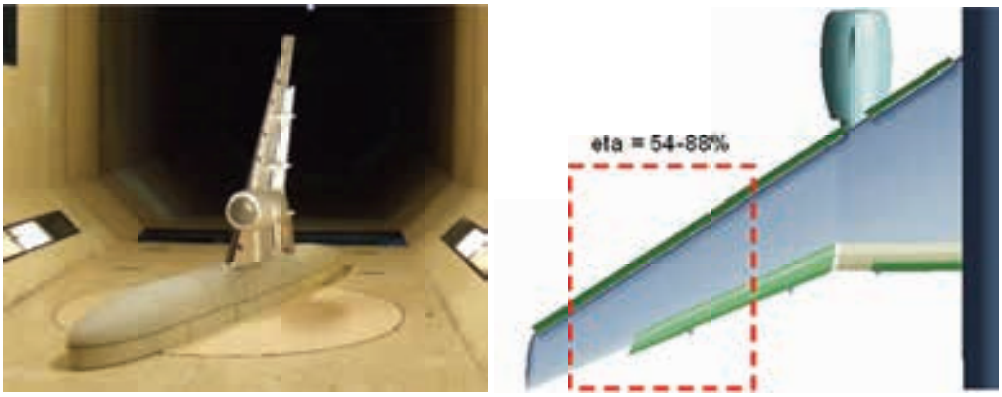

Fig. 7 JAXA high-lift device research model, "JSM"

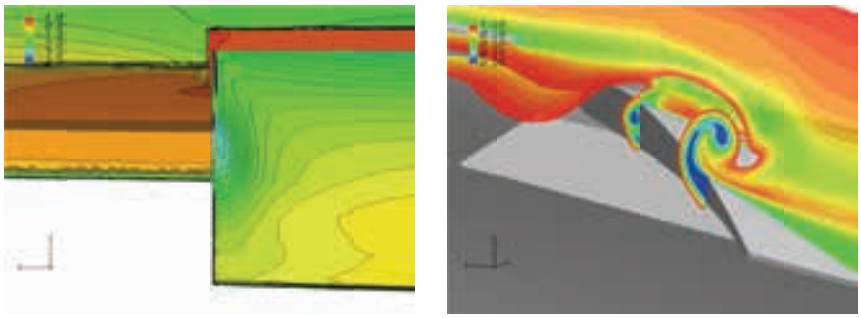

(a) Deployed in two-dimensional direction

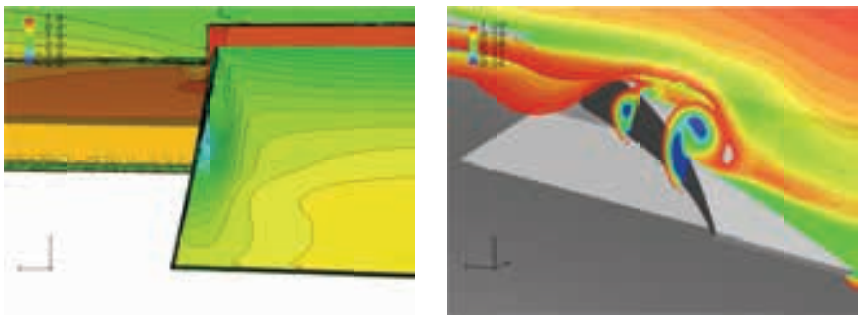

(b) Deployed in three-dimensional direction

Fig. 8 The difference of flowfields by the deployment methods of slat and flap preliminary evaluated by CFD (left: surface pressure distribution, right: total pressure loss)

If the load distribution of the JSM is reproduced on the model, it is expected that the model can reproduce the noise. Figure 9 shows the aerodynamic forces and moment of JSM measured in the wind tunnel test. Figure XXX indicates two results with different flap settings; (A) inboard single/outboard double flaps with 35deg deflection and (B) inboard/outboard single flaps with 30deg deflection. The lift coefficient at landing $C_{L(LD)}$ is estimated using C_{Lmax}.

$$V_{s1g} = \sqrt{2W/\rho S C_{Lmax}} \quad (1)$$

$$V_{L/D} = 1.23V_{s1g} = \sqrt{2W/\rho S C_{L(L/D)}} \quad (2)$$

$$C_{L(L/D)} = C_{Lmax}/1.23^2 \quad (3)$$

$C_{L(LD)}$ is estimated to be 1.89 and 1.84 and the corresponding angles of attack α are around 3°~4° and 5°~6° degrees for each flap setting.

Figure 10 compares the load distribution of JSM with inboard single/outboard double flaps with 35deg deflection at α=4° and the preliminary configuration of OTOMO2 obtained using CFD. In the preliminary configuration, the twist and dihedral angle are set to be zero. The load distribution of JSM from 54% to 88% span is re-scaled to be from 0% to 100%. Compared with the load distribution of JSM, it is confirmed that the load distribution of the preliminary configuration around 70% where the flap-edge is located shows good agreement at α=12° although the load distribution from 0% to 50% span is relatively lower. The load distribution will be adjustable to match better by considering twist distribution, while it complicates the model. Therefore, the twist distribution is not considered in the model.

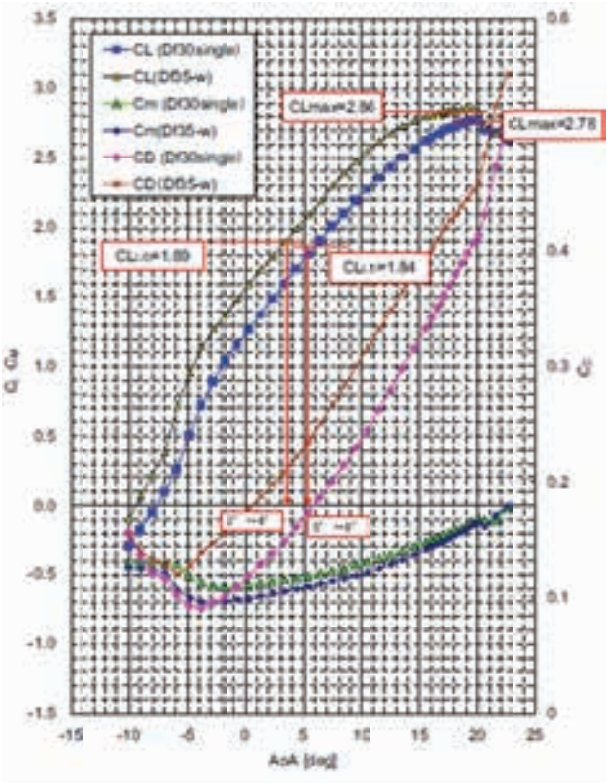

Fig. 9 Aerodynamic forces and moment of JSM measured in the wind tunnel test

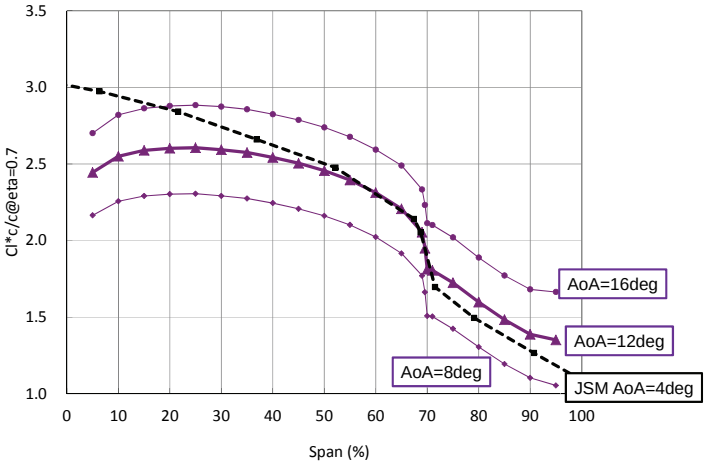

Fig. 10 Load distributions of JSM with inboard single/outboard double flaps with 35 deg deflection at α =4° from 54% to 88% span which is re-scaled to be from 0% to 100% and the preliminary configuration of OTOMO2 obtained using CFD

Model Sizing and Mounting in Wind Tunnel

As for the model sizing, the chord and span lengths of OTOMO are used for the baseline dimensions. The chord length and half wing span length are 0.6m and 1.35m. The stowed chord length at 70% span where the flap-tip locates is set to 0.6m. The appropriate scale is investigated based on the estimated amount of blockage and classical wind tunnel wall correction in JAXA-LWT2, the measurement frequency range, and the capacity to mount measurement sensors and tubes in the model. CFD simulation including wind tunnel of JAXA-LWT2 shown in Fig. 11 was used to validate the wind tunnel wall correction and to check the change of flowfields such as flow separation and vortices. To reduce the model scale to 80% from the baseline makes it difficult to mount all measurement sensors and tubes in the model. To increase the scale over 90% will increase the wind tunnel wall interferences compared with the results of OTOMO. Therefore, the model scale was decided to 85% scale of the baseline sizing. The angle of attack to be corrected is around 2° for the scale.

(a) Computational surface grid to simulate the model in JAXA-LWT2

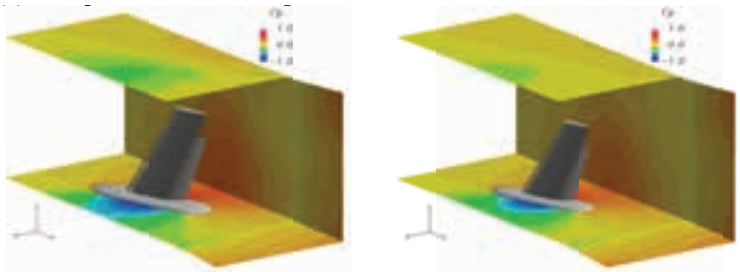

(i) Baseline model (ii) 85% scale model

(b) Comparison of surface pressure distribution on the wind tunnel walls

Fig. 11 Computations of the model in JAXA-LWT2 to investigate the wind tunnel wall interferences

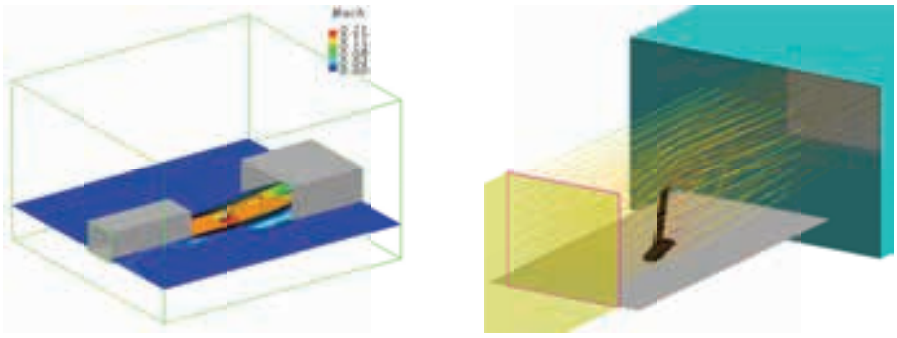

(a) Overview of computational domain and close-up view near the model

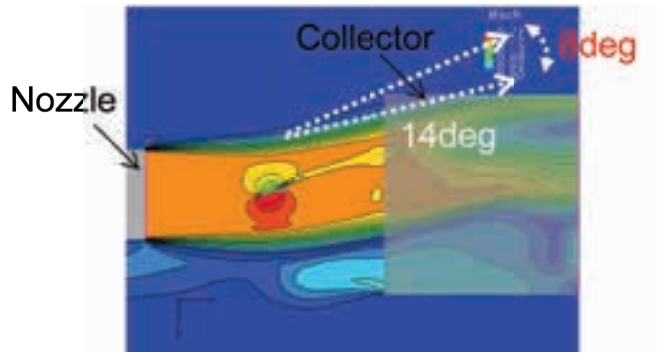

(b) Mach contours at 25% span section

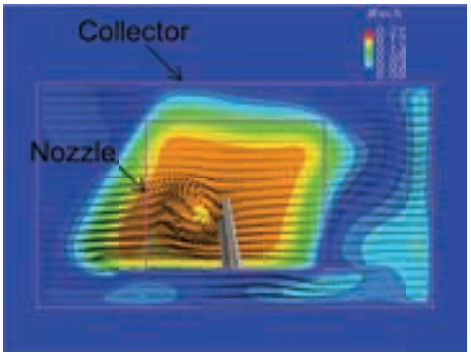

(c) Mach contours at the inlet of the collector

Fig. 12 Computation of the model in RTRI open-cart test section

In the case of open-cart test to measure the far-field noise, flow with shear-layer deflected due to high-lift has to be in the collector without generating extra noise at the required conditions. It was also evaluated by CFD. Figure 12 shows the computational results of the model in RTRI open-cart test section at α=16°. From the computational results, the flow is appropriately in the collector. The results also indicate the allowance to increase the angle of attack. These preliminary evaluations help to plan the wind tunnel test conditions and understand the test results.

In the half-span model testing mounted vertically on the wind tunnel, a spacer to avoid interferences between the model and the boundary layer of the bottom wind tunnel wall is often used. With less height of the boundary layer spacer, the inboard wing is influenced by the boundary layer interaction. The excessive height of the spacer increases lift and decrease drag. The careful selection of the height is important for half-span model tests. The appropriate height was evaluated by CFD. At a representative test condition in JAXA-LWT2, 99% height δ and displacement thickness δ^* of the floor boundary layer is 80mm and 7.5mm. Figures 13(a) and 13(b) shows the distribution of total pressure loss and surface pressure coefficients *Cp*. Figure 13(c) shows the influence on the spanwise load distribution. In Fig. 13(c), BL80 indicates the results with the floor boundary layer of δ=80mm. H20, H40 and H60 indicate that the height of the boundary layer spacer, H, are 20mm, 40mm and 60mm. In the computations, the floor boundary layer is modeled, but the wind tunnel itself is not simulated. As shown in Fig. 13(a), the floor boundary layer passes over the fuselage-like fairing and affects the inboard wing. In the case with H=20mm, the load reduces at a spanwise range from 5% to 30%. In the case with H=60mm, the load shows good agreement at 10%span, while increases at a spanwise range from 10% to 60%. From these observations, the height of the spacer was decided to be 40mm in JAXA-LWT2. Our previous computational and experimental studies using a realistic high-lift model, JSM, for high-lift aerodynamics research [31-32] had shown that a height of the spacer with the displacement thickness of the floor boundary layer δ^* or twice of δ^* is appropriate. For the present model, use of much thinner fuselage-like fairing requires much higher boundary layer spacer than the guideline.

The aft-part of the fuselage-like fairing was also modified by CFD considering the boundary layer spacer. Figure 14 shows the computational results with different aft-part of the fuselage-like fairing. The flow separation around the aft-part is reduced in the modifications. Space with height of 10*mm* is opened between the spacer and fuselage to exclude the measurement of the forces on the spacer. Then, a labyrinth seal is inserted in the space between the spacer and fuselage. The flow rate and flow speed passing through the labyrinth seal by the size of gaps were evaluated as shown in Fig. 15. Based on the observations, the labyrinth seal shown in Fig. 15(c) was selected.

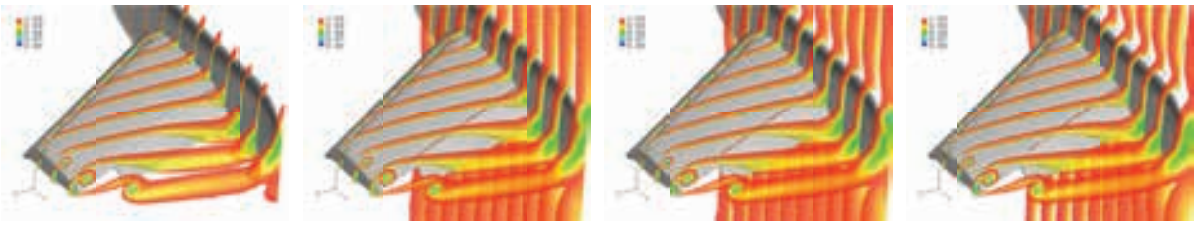

(i) δ=0mm, H=0mm (ii) δ=80mm, H=20mm (iii) δ=80mm, H=40mm (iv) δ=80mm, H=60mm

(a) Total pressure loss

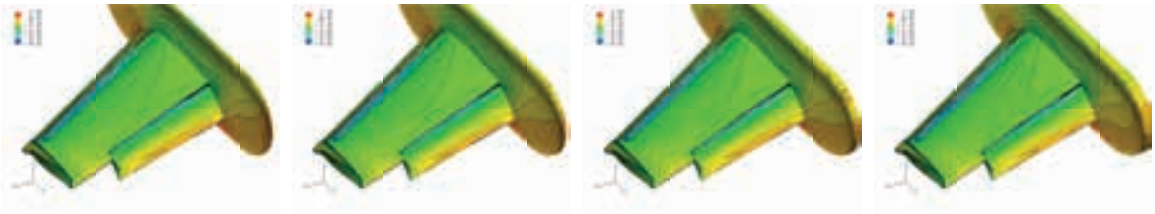

(i) δ=0mm, H=0mm (ii) δ=80mm, H=20mm (iii) δ=80mm, H=40mm (iv) δ=80mm, H=60mm

(b) Surface pressure distribution

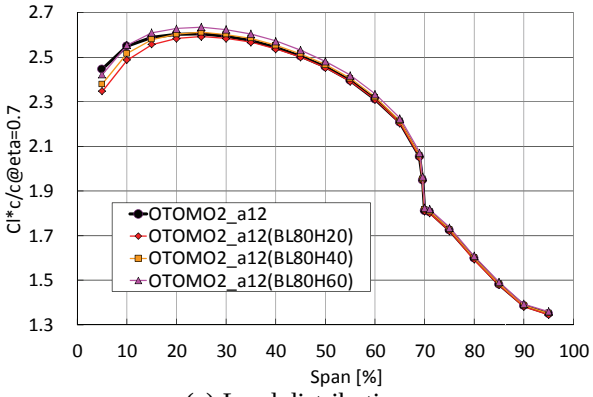

(c) Load distribution

Fig. 13 Evaluation of influence of the floor boundary layer with different height of the spacer at α = 12° (δ : 99% thickness of boundary layer, H: height of boundary layer spacer)

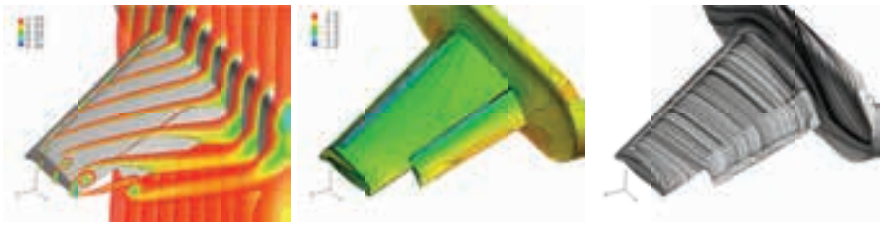

(a) Baseline fuselage-like fairing

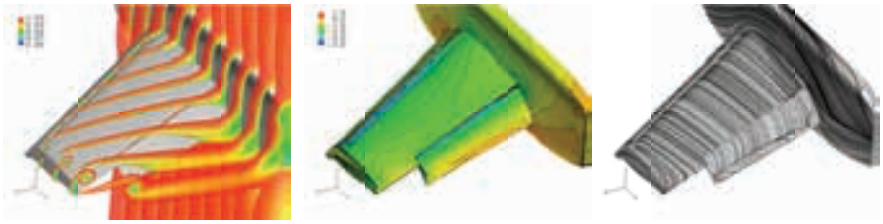

(b) Modified fuselage-like fairing

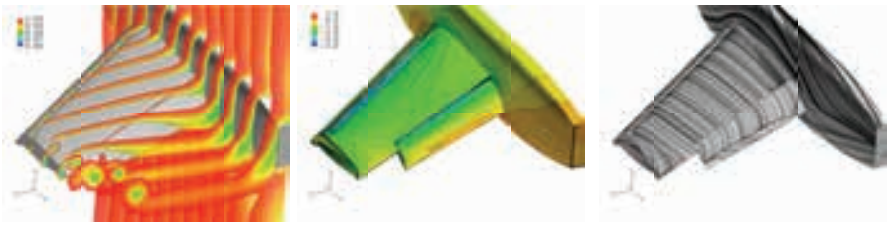

(c) Final fuselage-like fairing

Fig. 14 Evaluation of aft-part of fuselage-like fairing with boundary layer spacer at α = 12° (left: total pressure loss, center: surface pressure, right: surface restricted streamlines)

(i) ε=1mm (ii) ε=3mm

(a) Velocity contours at ΔP=1000Pa

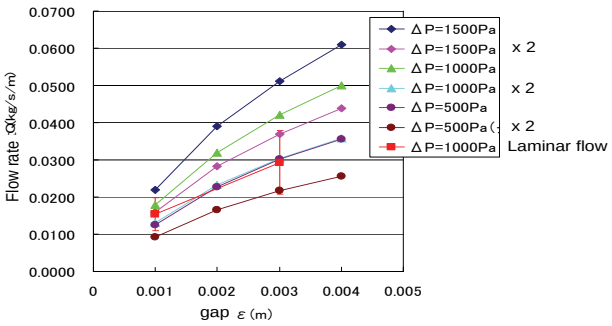

(b) Flow rate through the labyrinth seal

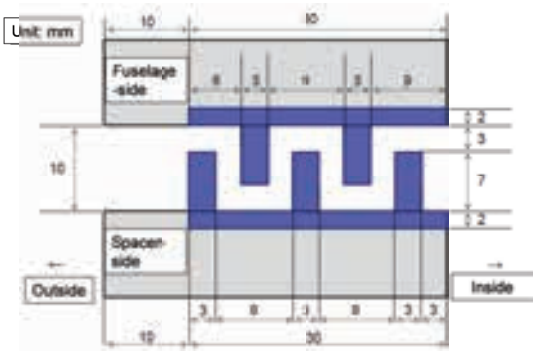

(c) Selected labyrinth seal

Fig.15 Design of labyrinth seal

Influences of Shear Layer and Mounted Plate on the Sound Propagation in Open-cart Test Section

In the case of open-cart test section, generated shear-layers largely deflect due to high-lift. For the purpose of high-lift device noise research, not only the wind tunnel data correction for aerodynamic forces, but also the influence on the sound propagation through the deflected shear-layers and sound reflection on the mounted plate should be evaluated. The influences were roughly evaluated using Linearized Euler Equations (LEE). Figure 16 shows a computational set-up to evaluate the sound reflection on the floor and structure to support the floor in the open-cart test section. A monopole sound source is set to a location. The location is changed from root to tip. Figures 17 and 18 show the influence of SPL by reflection on the floor and structure to support the floor for 500Hz and 1kHz sound sources, respectively. The results with the sound sources near the tip show more clear stripe pattern at X=0 section. By the location and frequency, the interferences are quite different.

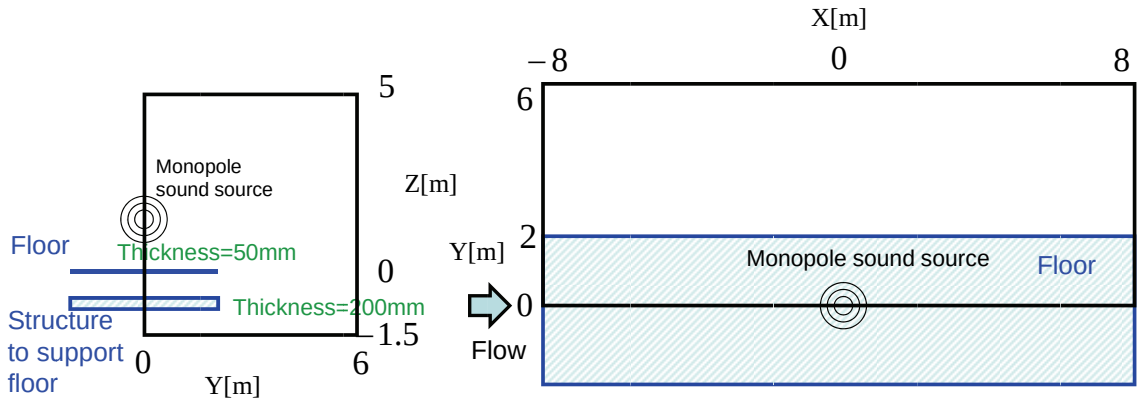

(a) View forward (b) view from top

Fig. 16 Computational set-up to evaluate the sound reflection on the floor and structure to support the floor

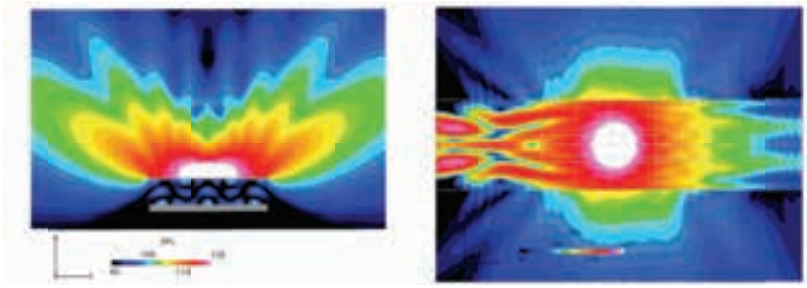

(i) X=0 (ii) Z=0

(a) Sound source at Z=145mm (root)

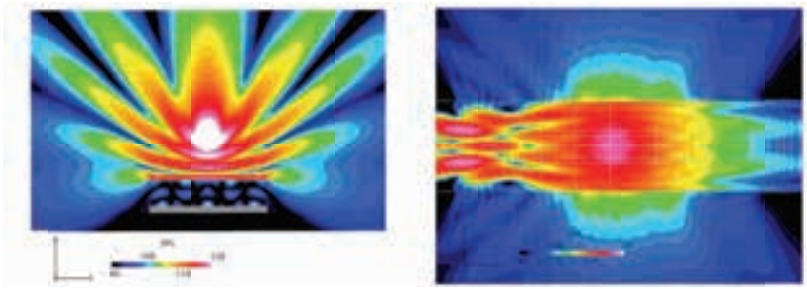

(i) X=0 (ii) Z=0

(b) Sound source at Z=1275mm (tip)

Fig. 17 Influence of SPL by reflection on the floor and structure to support the floor (monopole, 500Hz)

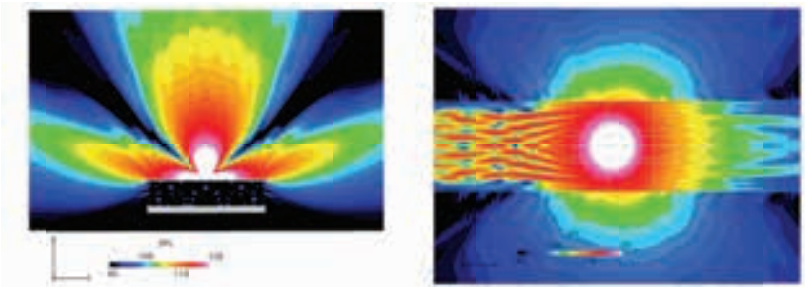

(i) X=0 (ii) Z=0

(a) Sound source at Z=145mm (root)

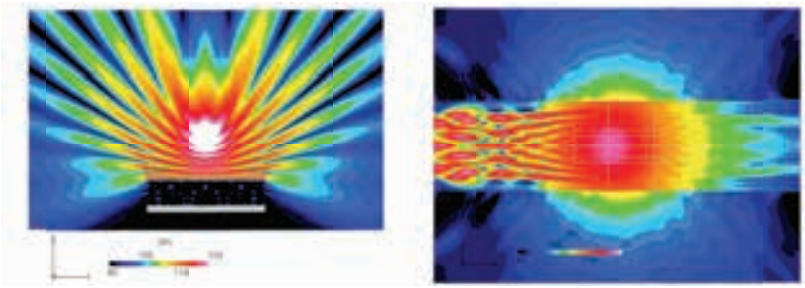

(i) X=0 (ii) Z=0

(b) Sound source at Z=1275mm (tip)

Fig. 18 Influence of SPL by reflection on the floor and structure to support the floor (monopole, 1000Hz)

Figure 19 shows computational set-up to evaluate influence on the sound propagation through the deflected shear-layers. CFD results shown in Fig. 12 are used as the background data for LEE. Figure 20 shows the influence of SPL by the wind tunnel flow. Figure 21 shows comparison of directivity change of SPL by the deflected shear-layers. Major influence is found in the downstream region. The influence is larger when the sound source locates near the tip. The difference is around 4dB at maximum. These data were compared with classical pressure correction methods. By the comparison, it turned that some parts of the influcences can be corrected by the classical method, while the downstream region can not be corrected. It is important to understand these characteristics for discussion of the real directivity of the noise removing wind tunnel interferences. The result is expected to contribute to sophisticate the classical correction method.

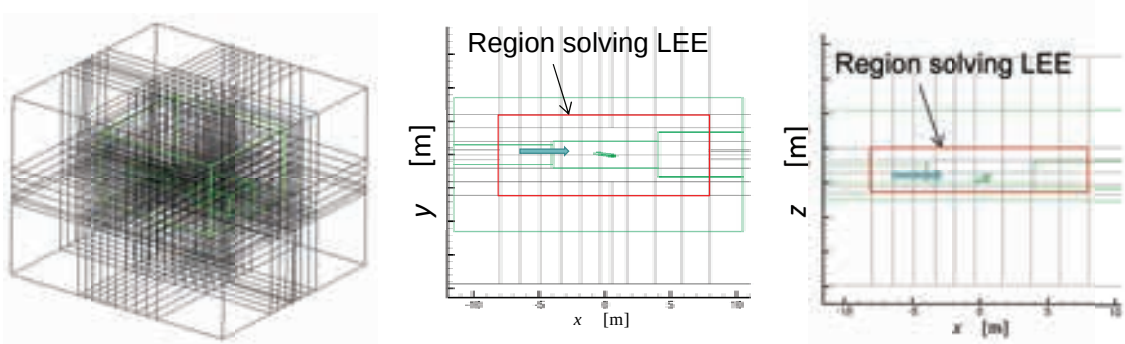

(a) Computational grid for LEE (b) Region solving LEE

Fig. 19 Computational set-up to evaluate influence on the sound propagation through the deflected shear-layers

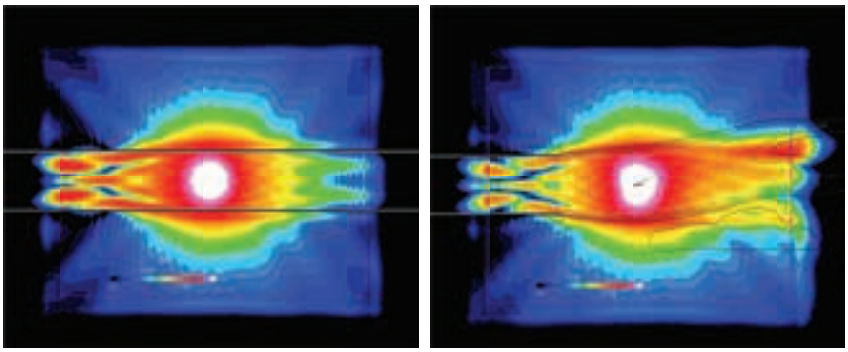

(i) Wind tunnel flow w/o model (ii) Wind tunnel flow w/ model
(a) Cross-section at Z=145mm (sound source at Z=145mm (root))

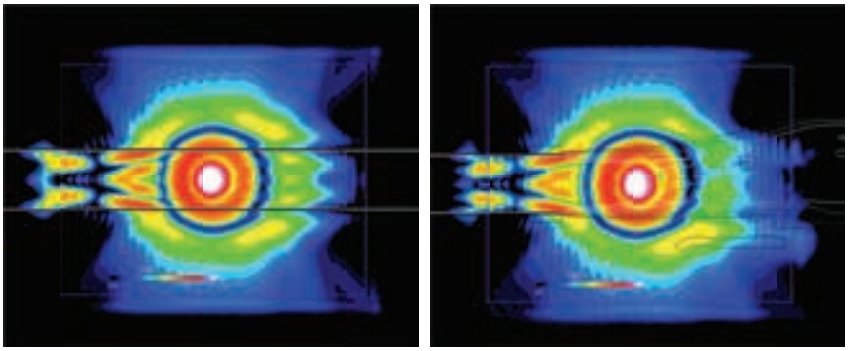

(i) Wind tunnel flow w/o model (ii) Wind tunnel flow w/ model
(b) Cross-section at Z=1275mm (sound source at Z=1275mm (tip))

Fig. 20 Influence on the sound propagation through the deflected shear- layers

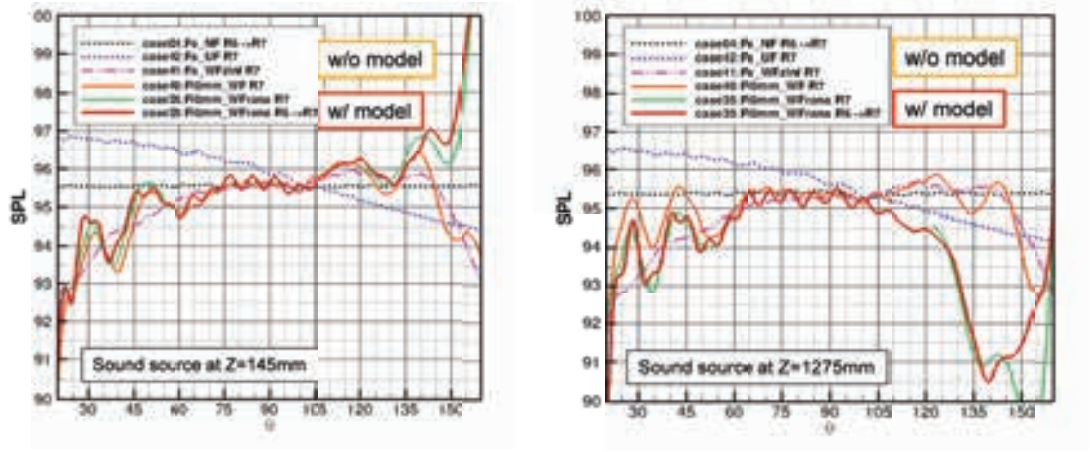

(a) Sound source at Z=145mm (root) (b) Sound source at Z=1275mm (tip)

Fig. 21 Comparison of directivity change of SPL by the deflected shear -layers

Concluding Remarks

Computational efforts in designing experiment for a series of wind tunnel tests of high-lift airframe noise measurement have been shown. The daily use of CFD/CAA towards airframe noise predictions especially for full aircraft configurations is still difficult and the airframe noise research relies largely on wind tunnel testing. For the airframe noise research, requirements of the accuracy of wind tunnel testing are severe. It has been

shown that preliminary CFD investigation of the wind tunnel tests can decrease unknowns and risks and improve the accuracy of the wind tunnel test. In the investigation, computations of a lot of configurations at many flow conditions had conducted with a limited schedule to design and fabricate the model, while improvement of the turnaround time of CFD would contribute to improve the wind tunnel test further. The continuing improvement and combination of CFD and EFD will be important for high-lift device noise research.

References

[1] Astley, J., "Predicting and Treating Fan and Turbomachinery Noise Current Technology, Research & Facilities," UK-Japan Bilateral Workshop (Aircraft Emissions and Noise), Tokyo, 2006.

[2] Hardin, J. C., "Airframe self-noise: Four years of research; aircraft noise reduction for commercial aircraft," NASA-TM-X-73908, 1976.

[3] Dobrzynski, W., "Almost 40 Years of Airframe Noise Research: What Did We Achieve?," *Journal of Aircraft*, Vol. 47, No. 2, 2010.

[4] Rudnik, R., and Geyr, H., "The European High Lift Project EUROLIFT II – Objectives, Approach, and Structure," AIAA Paper 2007-4296, Jun. 2007.

[5] Rumsey, C.L., Long, M., Stuever, R. A., and Wayman, T. R., "Summary of the First AIAA CFD High Lift Prediction Workshop," AIAA Paper 2011-0939, 2011.

[6] Murayama, M., Yokokawa, Y., Yamamoto, K., and Ueda, Y., "CFD Validation Study for a High-Lift Configuration of a Civil Aircraft Model," AIAA Paper 2007-3924, June 2007.

[7] https://info.aiaa.org/tac/ASG/FDTC/DG/BECAN_files_/Workshop_June_2010_Final_problem_Statements Contact_Information.pdf

[8] https://info.aiaa.org/tac/ASG/FDTC/DG/BECAN_files_/BANCII_Workshop_Announcement_051011.pdf

[9] Imamura, T., Ura, H., Yokokawa, Y., Enomoto S., Yamamoto K., Hirai, T., "Designing of Slat Cove Filler as a Noise Reduction Device for Leading-edge Slat," AIAA Paper 2007-3473, 2007.

[10] Imamura, T., Ura, H., Yokokawa, Y., Hirai, T., Yamamoto K., "Numerical and Experimental Research of Low-Noise Slat Using Simplified High-lift Model," AIAA Paper 2008-2918, 2008.

[11] Imamura, T., Yokokawa, Y., Ura, H., and Yamamoto, K., "A Far-field Noise and Near- field Unsteadiness of a Simplified High- lift- configuration Model (Slat)," AIAA Paper 2009-1239, 2009.

[12] Yokokawa, Y., Imamura, T., Ura, H., Ito T., Uchida, H., and Yamamoto, K., "Studies on Airframe Noise Generation at High-lift Devices in Relation to Aerodynamic Performances," AIAA Paper 2008-2960, 2008.

[13] Yokokawa, Y., Imamura, T., Ura, H., and Yamamoto, K., "A Far-field Noise and Near- field Unsteadiness of a Simplified High- lift- configuration Model (Flap-edge)," AIAA Paper 2009-283, 2009.

[14] Yamamoto, K., Imamura, T., Yokokawa, Y., "Progress on Experimental and Numerical Research for Slat Noise in JAXA," *International Journal of Aeroacoustics*, accepted.

[15] Murayama, M., Yokokawa, Y., Yamamoto, K., Imamura, T., and Ura, H., "Computational and Experimental Study on Noise Generation from Flap Side-Edge of a Simplified High-Lift Wing Model," Inter- Noise 2012, 2012.

[16] Yokokawa, Y., Murayama, M., Ito T., and Yamamoto, K., "Experiment and CFD of a High-Lift Configuration Civil Transport Aircraft Model," AIAA 2006-3452, 2006.

[17] Ura, H., Yokokawa, Y., Ito, T., and Yamamoto, K., "A Study of Airframe Noise from HLD by using Beamforming Techniques," Proceedings of 49th Aircraft Symposium, JSASS-2011-5103, 2011 (in Japanese).

[18] Streett, C. L., Lockard, D. P., Singer, B. A., Khorrami, M. R., and Choudhari, M. M., "In Search of the Physics: the Interplay of Experiment and Computation in Airframe Noise Research; Flap-Edge Noise," AIAA Paper 2003-977, 2003.

[19] Choudhari, M. M., Lockard, D. P., Macaraeg, M. G., Singer, B. A., Streett, C. L., Neubert, G. R., Stoker, R. W., Underbrink, J. R., Berkman, M. E., Khorrami, M. R., Sadowski, S. S., "Aeroacoustic Experiments in the NASA Langley Low-Turbulence Pressure Tunnel," NASA TM-2002-211432, 2002.

[20] Murayama, M. and Yamamoto, K., "Comparison Study of Drag Prediction by Structured and Unstructured Mesh Method," *Journal of Aircraft*, Vol.45, No.3, 2008, pp. 799-822.

[21] Yamamoto, K., Tanaka, K., Murayama, M., "Comparison Study of Drag Prediction for the 4th CFD Drag Prediction Workshop using Structured and Unstructured Mesh Methods," AIAA Paper 2010-4222, Jun. 2010.

[22] Takaki, R., Yamamoto, K., Yamane, T., Enomoto, S. and Mukai, J., "The Development of the UPACS CFD Environment," *High Performance Computing, Proceedings of the 5th International Symposium of ISHPC 2003*, edited by Vie-denbaum et al., Springer-Verlag, 2003, pp. 307-319.

[23] Imamura, T., Enomoto, S., Yokokawa, Y., and Yamamoto, K., "Simulation of the Broadband Noise from a Slat Using Zonal LES/RANS Hybrid Method," AIAA Paper 2007-0226, Jan. 2007.

[24] Nakahashi, K., Ito, Y., and Togashi, F, "Some challenges of realistic flow simulations by unstructured grid CFD", *International Journal for Numerical Methods in Fluids*, Vol.43, 2003, pp.769-783.

[25] Ito, Y. and Nakahashi, K. "Direct Surface Triangulation Using Stereolithography Data," AIAA Journal, Vol. 40, No. 3, pp. 490-496, 2002.

[26] Ito, Y. and Nakahashi, K., "Surface Triangulation for Polygonal Models Based on CAD Data," International Journal for Numerical Methods in Fluids, Vol. 39, Issue 1, pp. 75-96, 2002.

[27] Sharov, D. and Nakahashi, K., "A Boundary Recovery Algorithm for Delaunay Tetrahedral Meshing," Proceedings of 5th International Conference on Numerical Grid Generation in Computational Field Simulations, 1996, pp. 229-238.

[28] Ito, Y. and Nakahashi, K., "Improvements in the Reliability and Quality of Unstructured Hybrid Mesh Generation," International Journal for Numerical Methods in Fluids, Vol. 45, Issue 1, May 2004, pp. 79-108.

[29] Ito, Y., Shih, A., Soni, B., and Nakahashi, K., "An Approach to Generate High Quality Unstructured Hybrid Meshes," AIAA Paper 2006-0530, Jan. 2006.

[30] Maeda, T., and Kondo, Y., "RTRI's Large-scale Low-noise Wind Tunnel and Wind Tunnel Tests", Quarterly Report of RTRI, 2001, vol.42, no.2, pp.65-70.

[31] Murayama, M., Yokokawa, Y., Tanaka, K., Yamamoto, K., and Ito, T., "Numerical Simulation of Half-span Aircraft Model with High-Lift Devices in Wind Tunnel," AIAA Paper 2008-0333, Jan. 2008.

[32] Yokokawa, Y., Murayama, M., Uchida, H., Tanaka, K., Ito, T., and Yamamoto, K., "Aerodynamic Influence of a Half-Span Model Installation for High-Lift Configuration Experiment," AIAA Paper 2010-0684, Jan. 2010.